Palaeogeography, Palaeoclimatology, Palaeoecology 331–332 (2012) 150–161

Contents lists available at SciVerse ScienceDirect

Palaeogeography, Palaeoclimatology, Palaeoecology

journal homepage: www.elsevier.com/locate/palaeo

Eccentricity-paced late Paleozoic climate change

Daniel E. Horton [a,*], Christopher J. Poulsen [a], Isabel P. Montañez [b], William A. DiMichele [c]

[a] Department of Earth and Environmental Sciences, University of Michigan, Ann Arbor, Michigan 48109, USA
[b] Department of Geology, University of California, Davis, CA 95616, USA
[c] National Museum of Natural History MRC-121, Smithsonian Institution, Washington DC 20560, USA

ARTICLE INFO

Article history:
Received 24 April 2011
Received in revised form 7 March 2012
Accepted 10 March 2012
Available online 17 March 2012

Keywords:
Pangaea
Cyclothems
Milankovitch
Ice sheet response to climate
Cyclostratigraphy
Carbon dioxide
Orbital forcing
Late Paleozoic ice age
Tropical climate

ABSTRACT

Cyclic sedimentary deposits characterize low-latitude late Paleozoic successions and preserve evidence of dynamic climate change on the Pangaean supercontinent. Although their orbitally paced glacioeustatic origins are widely accepted, their climatic signatures are open to interpretation. In this study, we utilize the GENESIS general circulation model (GCM) coupled to dynamic ice sheet and ecosystem components, to explore the response of low-latitude continental climate and high-latitude ice sheets to orbital and atmospheric pCO_2 forcing. Our results suggest that atmospheric pCO_2 concentration exerts the primary control over low-latitude continental climate and high-latitude glaciation. Our experiments constrain the atmospheric pCO_2 window within which late Paleozoic climate was amenable to orbitally-driven glacial-interglacial fluctuations. The results suggest that both high-latitude ice-sheet accumulation and ablation and low-latitude climate change were paced by the eccentricity of Earth's orbit. Periods of high eccentricity amplified precession-driven changes in insolation and promoted high-latitude ice sheet volume fluctuations as well as increased low-latitude precipitation variability. When eccentricity was low, the amplification of precessionally-driven insolation fluctuations was reduced, which promoted high-latitude continental ice sheet stability and less variable low-latitude precipitation. Based on these modeling results we discuss the implications of eccentricity paced precessional-scale climatic changes on low-latitude Pangaean depositional environments.

1. Introduction

Climate change within the late Paleozoic Ice Age (LPIA; 320–260 Ma) was dynamic. Long-term (10^6-10^7 years) mean climatic states, hypothesized to be driven by fluctuations in greenhouse gas concentrations (Montañez et al., 2007) and the evolving configuration of continents about the South Pole (Crowell, 1978; Caputo and Crowell, 1985), alternated between icehouse and greenhouse conditions (Isbell et al., 2003; Fielding et al., 2008a; Fielding et al., 2008b). On shorter timescales (10^4–10^5 years) glacial-interglacial fluctuations are thought to have been driven by cyclic changes in Earth's orbit and associated feedbacks (Heckel, 1986; Horton et al., 2010). Geologic evidence of LPIA climate change is preserved within cyclic (~100 to 400 kyr) sedimentary deposits (i.e., cyclothems) that span paleo-equatorial Pangaea from the carbonate-dominated Bird Spring platform that rimmed the western tropical Panthalassic margin (Bishop et al., 2010; Martin et al., 2012), to the coal-rich sequences of the U.S. Mid-continent and Appalachian Basin (e.g., Cecil, 1990; Heckel, 2008), to the mixed paralic sequences of the Donets and Canadian Maritime basins that bordered the western Paleotethys (e.g., Gibling and Rygel, 2008; Eros et al., 2012). Cyclothem deposits throughout low-latitude Pangaea show considerable compositional variability, both regionally and temporally, but generally consist of repetitive lithological sequences whose stratigraphic facies variations record a wide range of depositional environments.

The periodic nature of low-latitude late Paleozoic sequences was originally hypothesized to result from orbitally-driven glacioeustatic changes associated with the waxing and waning of high-latitude Gondwanaland ice sheets at eccentricity frequencies (100 and 400 kyr), analogous to Milankovitch's theory of orbital control of Northern Hemisphere ice sheets during the Pleistocene (Heckel, 1986). While glacioeustatic changes explained some of the observed lithofacies variations found in late Paleozoic cyclic deposits it became apparent that other factors, notably changes in the climatic conditions within the depositional environment, were also at work. Subsequently, it was proposed that variations in low-latitude climate, driven by changes in high-latitude ice volume, controlled both the delivery of sediment to, and the geochemical conditions within, disparate depositional environments and could, in conjunction with glacioeustatic change, better explain cyclothem lithofacies variations across a wide range of depositional settings (Cecil, 1990; Cecil et al., 2003). Multiple orbitally paced glacioeustatic/climate change deposition models have since been proposed (e.g., Soreghan, 1994; Tandon and Gibling, 1994; Heckel, 1995; Miller et al., 1996; Rankey, 1997) with considerable

* Corresponding author now at: Department of Environmental Earth System Science, Stanford University, 473 Via Ortega, Stanford, CA 94305–4216. Tel.: +1 734 709 1730.
E-mail addresses: danethan@stanford.edu (D.E. Horton), poulsen@umich.edu (C.J. Poulsen), ipmontanez@ucdavis.edu (I.P. Montañez), dimichel@si.edu (W.A. DiMichele).

0031-0182/$ – see front matter © 2012 Elsevier B.V. All rights reserved.
doi:10.1016/j.palaeo.2012.03.014

disagreement as to the synchroneity of changing ice volumes (and by corollary, eustasy) and the low-latitude climate changes that are hypothesized to result (cf. Rankey, 1997). Moreover, these deposition models generally fail to consider the direct effects of insolation change on low-latitude climate.

In this study we utilize a coupled atmosphere-ice sheet-vegetation model to investigate the influence of dynamic orbital configurations and atmospheric pCO_2 on low-latitude Pangaean climate and high-latitude Gondwanaland glaciation. Our results indicate that atmospheric pCO_2 concentration exerts the primary control on high-latitude late Paleozoic continental ice sheets and low-latitude precipitation. Our results further indicate that orbital insolation variations are sufficient to drive significant variability in low-latitude continental climate without the influence of ice sheets. Finally, we identify a pCO_2 window within which high-latitude late Paleozoic ice sheets remain sensitive to changes in orbital insolation. Using our climate modeling results, we develop a mechanistic model that is applicable to cyclothemic successions throughout the Pangaean paleotropics, and links both high-latitude glacial-interglacial fluctuations and low-latitude climate change to variations in the eccentricity of Earth's orbit about the Sun.

2. Model and methods

The results presented in this manuscript are based on model simulations that were previously discussed in Horton et al. (2010). In that manuscript, the results mainly focused on high-latitude climate interactions. In this study we incorporate the findings presented in Horton et al. (2010), but expand our focus to incorporate low latitude climate change and more thoroughly examine the late Paleozoic climate system.

To investigate LPIA climates we utilize the GENESIS Earth system climate model coupled to dynamic ecosystem and ice sheet modeling components. The GENESIS version 3.0 general circulation model has been used extensively for paleoclimatic simulations and is comprised of atmospheric, land-surface, sea-ice, and 50 m slab-ocean components (Pollard and Thompson, 1995; Thompson and Pollard, 1995, 1997). The GENESIS atmosphere is run with a T31 spectral resolution (3.75°×3.75°) and 18 vertical levels. The land surface model resolution is 2°×2° and utilizes a Sakmarian paleogeographic/paleotopographic reconstruction (~290 Ma; Ziegler et al., 1997). The 50 m slab-ocean does not simulate changes in sea level, thus climatic changes brought about by changing sea level cannot explicitly be addressed. We synchronously couple GENESIS to the BIOME4 ecosystem model, an equilibrium vegetation model that predicts global biome distributions and plant physiology based on monthly average temperature, precipitation, insolation, and pCO_2 concentration. BIOME4 was developed from the BIOME ecosystem modeling lineage with the intent to capture more accurately the distribution of high latitude ecosystems thought to have existed during the ice house conditions of the last glacial maximum (Harrison and Prentice, 2003; Kaplan et al., 2003). Since the grassland ecosystem had not yet evolved in the late Paleozoic, we exclude it (Strömberg, 2005). The three-dimensional ice sheet model is asynchronously coupled to the GENESIS-BIOME4 modeling scheme because the response time of the atmosphere and ice sheets differs by two orders of magnitude. The thermomechanical ice sheet model utilizes GCM-derived climatic data and is based on the vertically integrated continuity equation for ice mass balance. The evolution of continental ice sheet geometry is simulated via surface mass balance, basal melting, and ice-flow calculations on a 1°×2° surface grid (DeConto and Pollard, 2003).

The results presented in this manuscript address changes brought about by (1) differences in the mean climate state as well as (2) short-term orbitally driven transient climate variations. Previous modeling studies have suggested that late Paleozoic mean climatic states, e.g. glacial, interglacial, and ice-free climates, are largely controlled by the concentration of pCO_2 in the atmosphere (Horton et al., 2007, 2010; Horton and Poulsen, 2009). In accord with these results, the mean climate states simulated in our experiments correspond to a range of pCO_2 concentrations; (a) relatively stable glacial conditions at 420 ppm, (b) glacial-interglacial fluctuations at 560 ppm, and (c) largely ice-free conditions at 840 ppm. To capture the transient evolution of climate due to short-term orbital parameter variation within each mean climatic state we utilize a coupling scheme that consists of alternating short (15 years) GCM-biome integrations and long (5 kyr) ice-sheet integrations. Between the integration of each component, updated boundary conditions (e.g. meteorological information to the ice-sheet model or ice geometry to the GCM-biome model) are passed from one model component to the other, and orbital parameters are updated. For computational efficiency, we have simplified the periods of each orbital parameter such that eccentricity, obliquity, and precessional periods occur every 80, 40, and 20 kyrs, respectively; an action that reduces complex interference patterns, but ensures extremes in insolation distribution (See Section 4.3 for more discussion; DeConto and Pollard, 2003; Horton and Poulsen, 2009). Each transient experiment began with ice-free continents and was run through three orbital cycles (80 kyrs each), for a total of 240 kyrs (48 iterations).

For analysis purposes, the mean climate of each individual (15 years) time slice is calculated by averaging the final five years of each GCM iteration. Using these time slice averages, this study presents results in two different formats. (1) To examine the role of mean climatic states, the transient orbital scheme is subdivided into three 80 kyr (eccentricity cycle) segments, termed Orbit 1 (1–80 kyr), Orbit 2 (81–160 kyr), and Orbit 3 (161–240 kyr; Fig. 1a). Each 80 kyr segment was compiled using the same orbital forcing sequence and the mean climate of each 80 kyr segment is calculated by averaging the annual mean of all constituent time slices. (2) To examine the role of dynamic orbital forcing in the low latitudes, we separately averaged climate parameters over the northern and the southern (0°–15°) terrestrial tropics and concatenated each time slice's average into a 240 kyr time series.

3. Results

3.1. Ice sheet behavior

In our simulations, ice sheet area, volume, and equatorward extent are largely controlled by the atmospheric pCO_2 concentration and its effect on global mean temperature. In the 420-ppm simulation, the global average ice sheet volume increases from 1.93×10^7 km^3 to 7.70×10^7 km^3 over three orbital cycles (black line; Fig. 1a). In southern Gondwanaland, a single supercontinental ice sheet accumulates and expands northward to 48° S, eventually covering 2.65×10^7 km^2 of the continent's surface and attaining an average height in excess of 2900 m (Fig. 1b). This ice sheet contains the water-equivalent of ~179 m of sea-level change, a value approaching the maximum estimates reported for high-frequency glacioeustasy in the late Paleozoic (Rygel et al., 2008). In the 560-ppm simulation, global average ice sheet volume increases from 6.88×10^6 km^3 to 1.75×10^7 km^3 over the three orbital cycles (blue line; Fig. 1a). In Gondwanaland, multiple ice sheets form and at their maximum reach northward to 65° S and cover 1.11×10^7 km^2 of the continent's surface (Fig. 1c). In the 840-ppm simulation, Gondwanaland is largely ice free (red line; Fig. 1a), though isolated low-volume (5.93×10^6 km^3 maximum) ice deposition centers form along the Panthalassan coast in the extreme high southern latitudes (Fig. 1d).

In our simulations, ice sheets demonstrate the greatest response to orbital insolation fluctuations when the eccentricity of Earth's orbit is high. High eccentricity amplifies precessional changes in insolation and leads to summer temperature maxima and minima in the

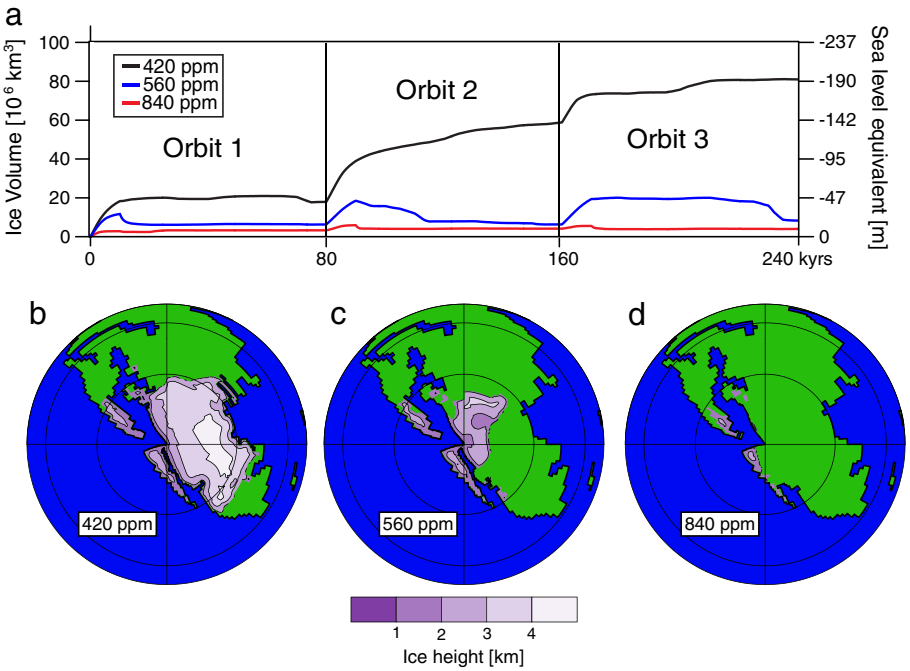

Fig. 1. Time-series and time-slices of simulated late Paleozoic ice sheets. (a) Global ice volume and equivalent sea-level change time-series for each pCO_2 experiment (modified from Horton et al., 2010). Orbits 1–3 refer to periods that have been averaged to determine mean climatic states (for full description see Section 2). (b–d) Late Paleozoic (~290 Ma; Ziegler et al., 1997) southern hemisphere polar projection snapshots (170 kyr) of Gondwanaland ice sheets at each atmospheric pCO_2 concentration. The latitudinal contour interval is 30°.

high latitudes. Significant ice sheet volume increases occur during anomalously cold southern hemisphere summer orbits (high eccentricity, low obliquity, and SH summer solstice at aphelion), whereas ice sheet volume decreases coincide with anomalously warm SH summer orbits (high eccentricity, low obliquity, and the SH summer solstice at perihelion; Fig. 1 in Horton et al., 2010). At pCO_2 concentrations of 420 ppm, an ice sheet volume reduction is simulated at the end of Orbit 1, but thereafter the ice sheet grows sufficiently large to be insensitive to orbitally-induced warming due to the cooling effects of ice height and albedo feedbacks (black line; Fig. 1a). At pCO_2 concentrations of 560 ppm, the ice sheet waxes and wanes (by up to 33 m in sea-level equivalent) in response to orbital insolation fluctuations (blue line; Fig. 1a). This response varies throughout the 240-kyr simulation due to the initialization of our experiments with ice-free boundary conditions and the interaction of ecosystems and climate at the ice sheet margin (Horton et al., 2010).

3.2. Effect of ice sheets on precipitation

The ice sheets simulated in our experiments have little to no influence on Pangaean mean-annual precipitation or wet-season length (Fig. 2a–r). For each pCO_2 level the net effect of ice sheet growth on precipitation is determined by comparing the average climate early in the simulation period (Orbit 1) to the average climate late in the simulation period (Orbit 3), when substantial ice sheet volumes have accumulated. Changes in mean-annual precipitation greater than ± 1 cm/month are observed in the high latitudes of the 560- and 420-ppm experiments due to the orographic effect of ice sheets and within an isolated region of mid-continent tropical Pangaea at 420 ppm (Fig. 2c). Changes in the length of low-latitude wet-seasons, measured here as the number of months per year with precipitation in excess of 10 cm, occur in isolated pockets at all simulated pCO_2 levels, though it should be noted that such changes rarely exceed ± 1 month/year in wet-season length (Fig. 2j–r).

In previous late Paleozoic climate modeling studies using similar modeling components, it was found that the addition of prescribed Gondwanaland ice sheets led to significant precipitation changes in tropical Pangaea (Poulsen et al., 2007; Peyser and Poulsen, 2008). These studies attributed the change in low-latitude precipitation to ice sheet induced strengthening of the low-latitude temperature gradient, which, in turn, intensified Hadley cell overturning. The prescribed ice sheet geometries, which include ice height and areal extent, used in these studies were based on mapped glacial remnant deposits (including ice-rafted debris) and in some cases represent "extreme" ice-coverage estimates (in one simulation ice extends from the pole to 20° S). Our results in this study differ from those presented in these previous studies because we use a dynamic ice sheet model that predicts ice sheet geometries based on simulated climatology, which results in ice sheets that are taller and less extensive than those prescribed in the Poulsen et al. (2007) and Peyser and Poulsen (2008) studies. Because our ice sheets do not extend as far northward as those prescribed in these previous studies, the low-latitude temperature gradient increase is comparatively reduced, as is the strength of the Hadley circulation (compare Fig. 3b-c of this paper with Fig. 6 in Peyser and Poulsen). In our present experiments, low-latitude Pangaea cools by an average of ~1 °C due to the accumulation of ice from Orbit 1 to Orbit 3 in the 420-ppm experiment (Fig. 3a). This low-latitude cooling slightly intensifies the Hadley overturning circulation (Fig. 3b–c) and is responsible for the small increase in mean-annual precipitation noted above in Fig. 2c.

3.3. Mean climatic state effect on tropical precipitation

Our results indicate that the dominant influence on tropical continental precipitation is the global mean temperature, as determined by the atmospheric pCO_2 concentration. To analyze the effect of global mean temperature on tropical continental precipitation, we compare the mean Orbit 3 climate of the 420- and 560-ppm simulations to that of the 840-ppm experiment. In all comparisons tropical mean-annual precipitation over land is greater in the lower pCO_2 simulations (Fig. 4a and c), while over the oceans precipitation decreases with

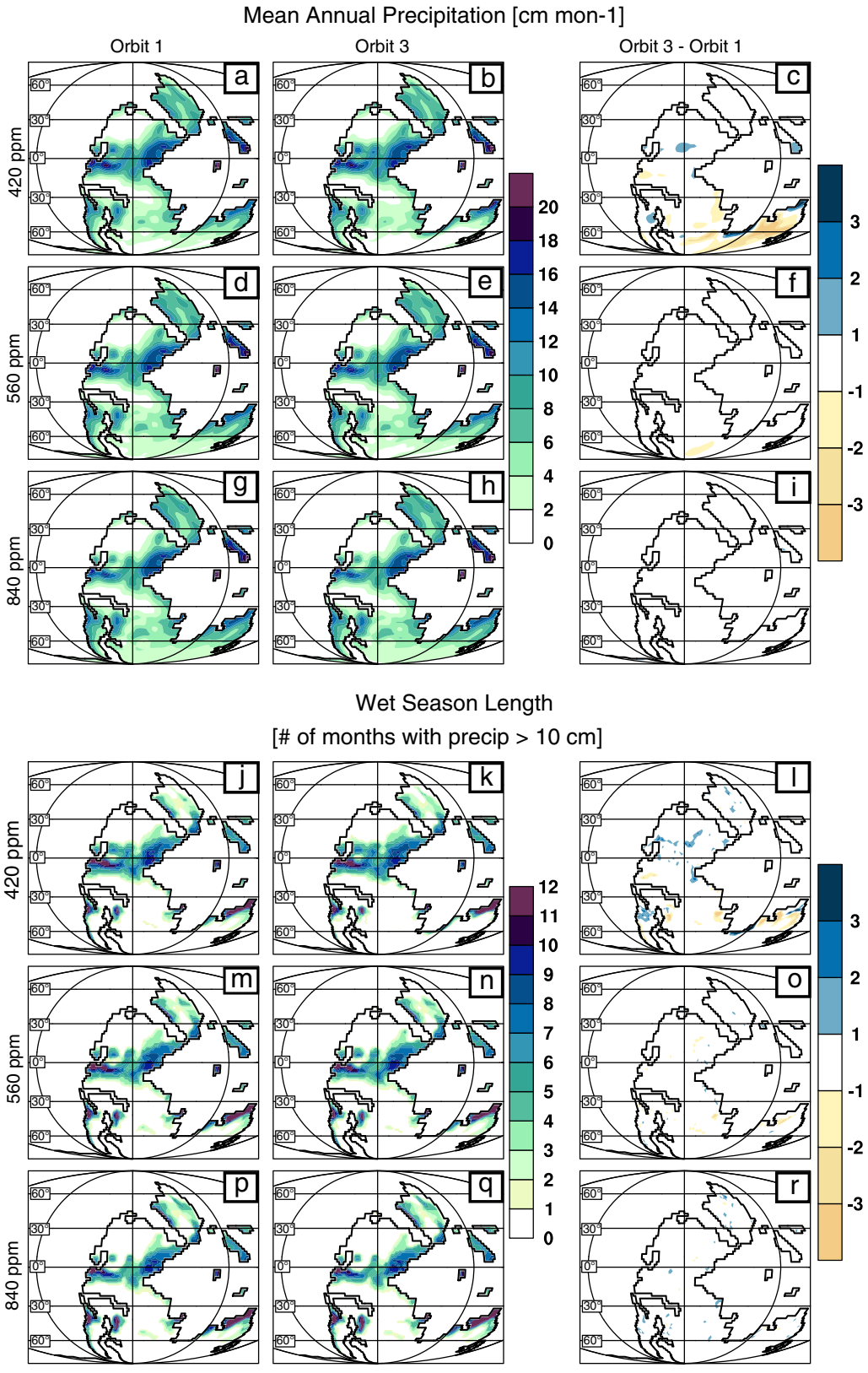

Fig. 2. Mean annual precipitation (a–i) and wet-season length (j–r) simulated at each pCO_2 concentration. Orbit 1 average in left column, Orbit 3 average in middle column, and Orbit 3 — Orbit 1 difference plots in right column. Wet-season length is defined as the number of months per year that precipitation exceeds 10 cm.

lower pCO_2 concentrations (Supplementary Fig. 1). In the 420–840 ppm comparison, mean-annual precipitation throughout the majority of the continental tropics is up to 6 cm/month higher in the lower pCO_2 experiment (Fig. 4a). In conjunction with increased precipitation, the number of months in which precipitation exceeds 10 cm increases by an average of 1 to 5 months per year and the tropical wet-season length increases (Fig. 4b). Mean-annual precipitation and wet-season length differences between the 560- and 840-ppm experiments show similar

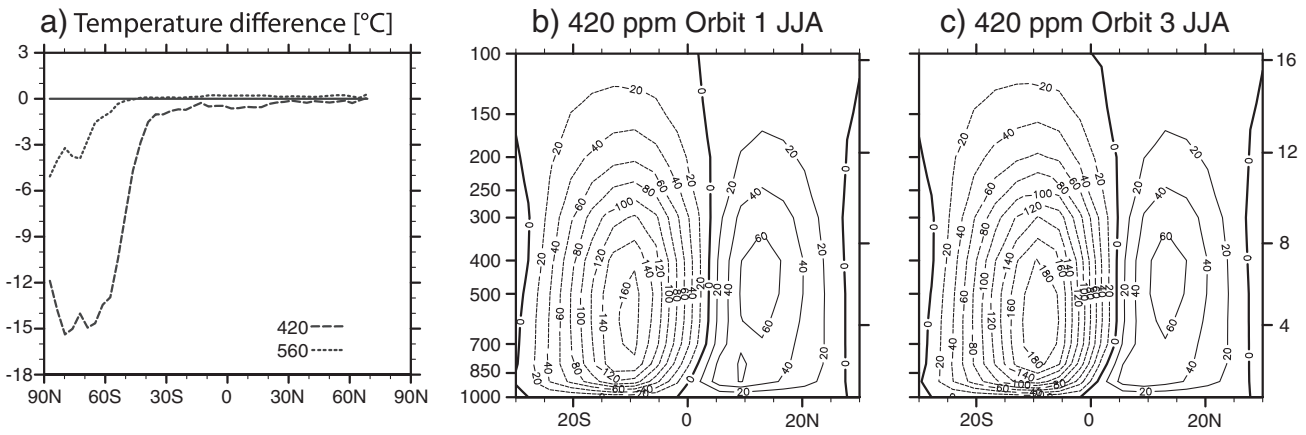

Fig. 3. Zonal temperature difference and atmospheric circulation. (a) Continental temperature differences (Orbit 3–Orbit 1) for 420 and 560 ppm atmospheric pCO_2 concentration experiments. (b–c) The June–July–August (JJA) meridional overturning streamfunction for average 420 ppm Orbit 1 (b) and Orbit 3 (c) climates [10^9 kg s^{-1}]. On each plot (b-c) the left y-axis is pressure [mb] and the right y-axis is height [km].

trends to the 420–840 ppm comparison, though the magnitude of differences is smaller (Fig. 4c–d).

According to the Clausius–Clapeyron (CC) relation, higher greenhouse gas concentrations increase the saturation vapor pressure of the atmosphere, leading to enhanced precipitation and evaporation. Consistent with the CC relation, precipitation over the oceans increases with increasing pCO_2 concentration, and is reduced with declining pCO_2. Over the Pangaean super-continental tropics however, precipitation decreases with increasing atmospheric pCO_2 due to higher temperatures, increased water stress, and ultimately the expansion of desert and xerophytic ecosystems at the expense of forest, shrubland, and/or savanna ecosystems (Fig. 5). The low vegetation density in desert and xerophytic ecosystems reduces soil moisture and leads to lower precipitation rates (Poulsen et al., 2007). At lower pCO_2 concentrations, densely vegetated ecosystems expand within the tropical latitudes, increasing soil moisture, evapotranspiration, and precipitation. Throughout the 240-kyr simulation, vegetation coverage and mean-annual precipitation are positively correlated (Fig. 6). The role of vegetation is further established by a comparison of vegetated and desert/xerophytic low-latitude model grid cells, which indicates that areas with vegetated land cover receive ~70% more precipitation than desert/xerophytic regions (Fig. 7d and f).

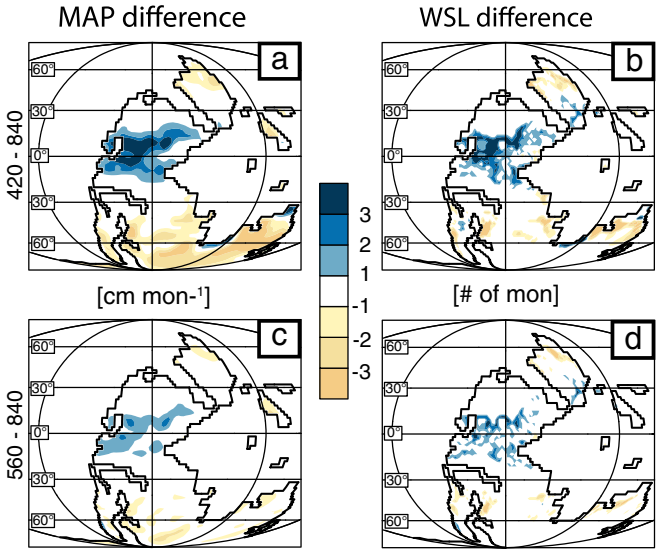

Fig. 4. Orbit 3 difference plots of mean annual precipitation (MAP in cm mon^{-1}; a and c) and wet-season length (WSL in number of months; b and d). pCO_2 difference plots are calculated by subtracting the 840 ppm climatic conditions from those simulated at 420 and 560 ppm. Climatic conditions over the oceans have been masked (for an unmasked version, see Supplementary Fig. 1).

3.4. Orbital variability at low latitudes

Changes in Earth's tilt, season of perihelion, and the degree to which Earth's orbit about the Sun is eccentric influence the amount and distribution of insolation, and alter global temperatures and precipitation patterns (Imbrie and Imbrie, 1980). In our late Paleozoic

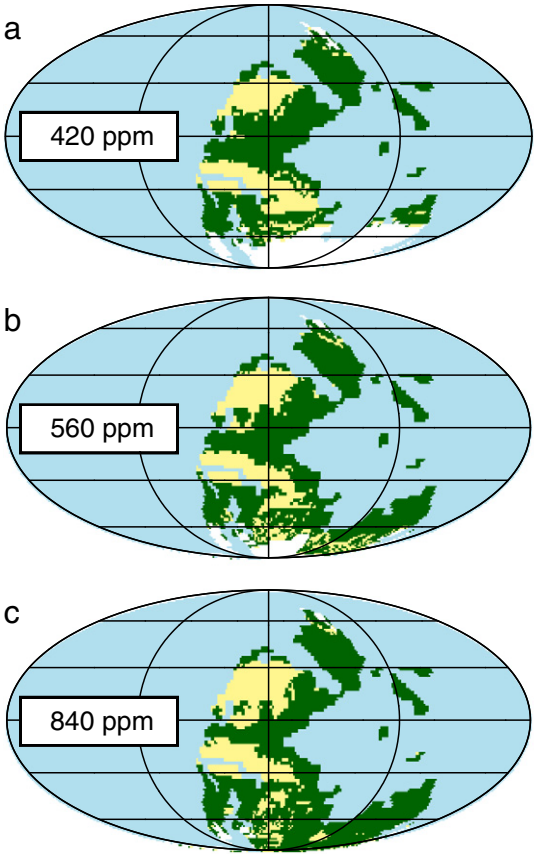

Fig. 5. Orbit 3 mean vegetation distributions; (a) 420, (b) 560, (c) 840 ppm. Desert, barren, and xerophytic shrublands are depicted in yellow. All other ecosystems are green. Continental ice sheets are white and oceans/seas are blue. The latitudinal contour interval is 30°.

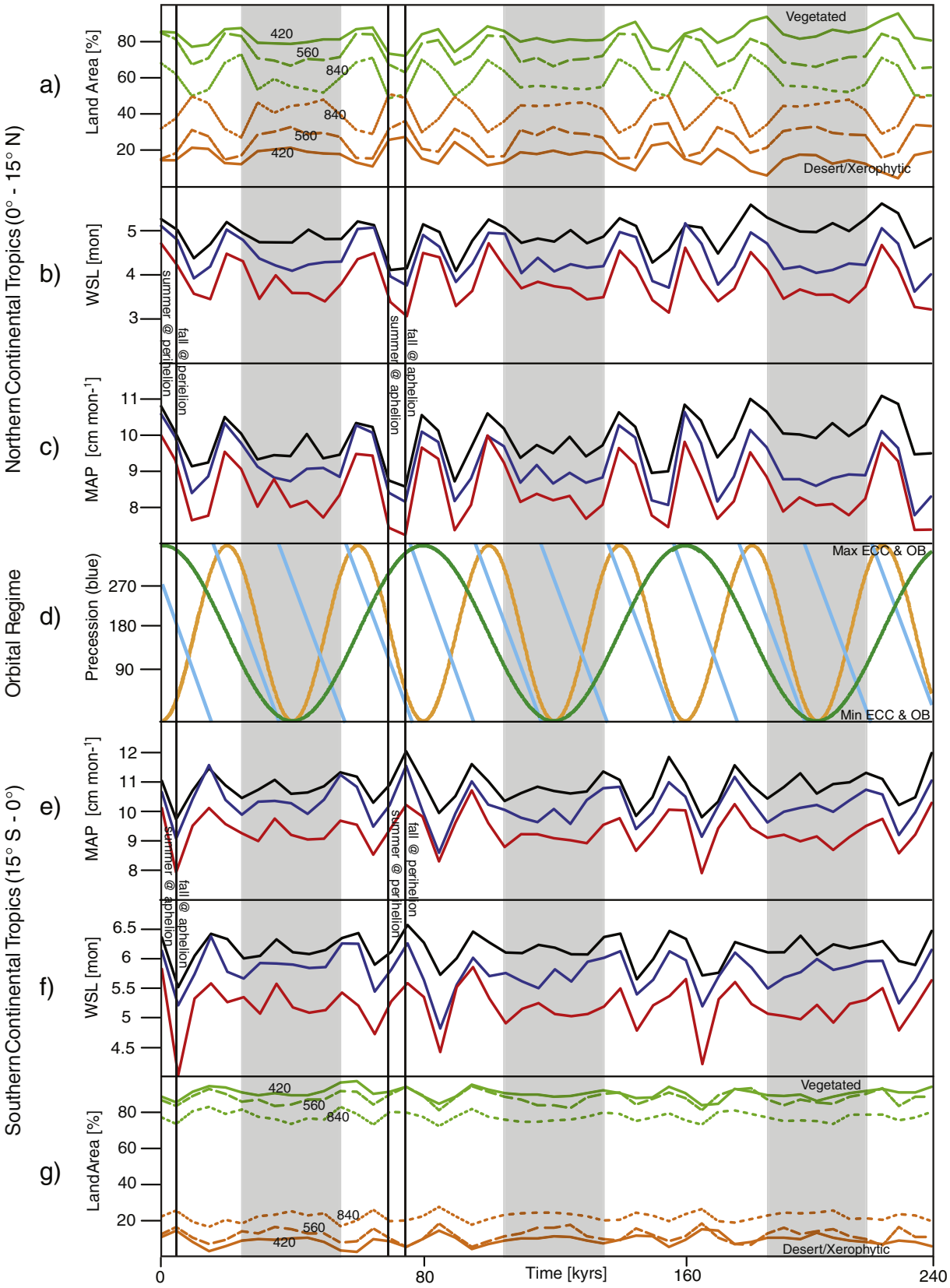

Fig. 6. Time-series of continental low-latitude climate parameters shown by hemisphere. The percentage of Pangaea covered in desert/xerophytic or other (vegetated) ecosystems (a and g), wet-season length (WSL; b and f), and mean-annual precipitation (MAP; c and e) in both the northern (a–c) and southern hemisphere (e-g) tropics (0°–15° S and 0°–15° N). WSL and MAP plots depict climatic conditions at different pCO_2 concentrations (420 ppm in black, 560 ppm in blue, and 840 ppm in red). (d) The simulated orbital regime used in our experiments; values are based on Plio-Pleistocene maxima and/or minima (Berger and Loutre, 1991). Precession (light blue in d) is measured as the angle between northern hemisphere vernal equinox and perihelion. Eccentricity (ECC; green in d) ranges from a maximum of 0.057 to a minimum of 0.0002. Obliquity (OB; orange in d) ranges from 24.538° to 22.079°. Thick vertical gray bars highlight periods of low eccentricity. Thin vertical black lines highlight examples of different seasons at aphelion/perihelion during periods of high eccentricity.

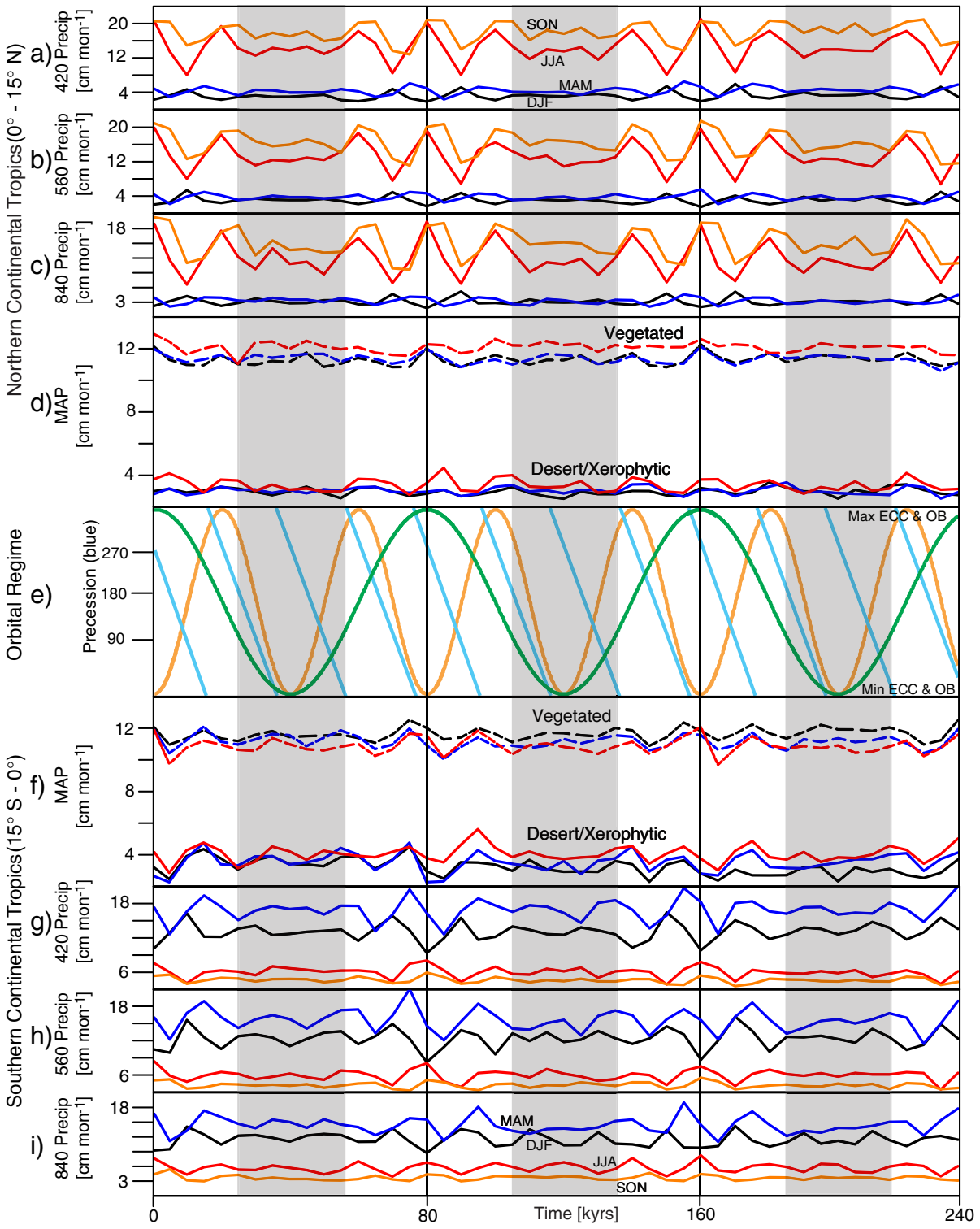

Fig. 7. Time-series of continental precipitation shown by hemisphere. (a–c) Low-latitude northern hemisphere (NH; 0°–15° N) seasonal precipitation for each pCO_2 level experiment (DJF: December–January–February, MAM: March–April–May, JJA: June–July–August, SON: September–October–November). Note change in precipitation axis for 840 ppm experiment. (d) NH mean-annual precipitation in vegetated versus desert/xerophytic grid cells for each simulated pCO_2 concentration (420 ppm in black, 560 ppm in blue, and 840 ppm in red). (e) Orbital regime used in simulations (See Fig. 6 caption). (f) Low-latitude southern hemisphere (SH; 0°–15° S) mean-annual precipitation for vegetated versus desert/xerophytic grid cells for each simulated pCO_2 concentration. (g–i) SH seasonal precipitation for each pCO_2 level. Note change in axis for 840 ppm experiment. Thick vertical gray bars highlight periods of low eccentricity.

simulations, tropical continental precipitation exhibits the greatest variability during periods of high eccentricity and less variability during periods of low eccentricity (Fig. 6c–e). When Earth's orbit about the Sun is eccentric, precession-driven temperature variations are amplified and the variability of seasonal precipitation increases, i.e., maxima in precipitation seasonality is followed shortly thereafter (10 kyr) by minima (Figs. 6 and 7). As the eccentricity of Earth's orbit is reduced, the amplification of precessional insolation changes weakens, and seasonal variability declines. Within the latitudes from which known cyclothems formed (~15° S to 15° N), mean-

annual precipitation is dominated by the summer/fall wet-season. When a given hemisphere's wet-season occurs during perihelion (aphelion) and Earth's orbit is eccentric, the insolation-driven temperature increase intensifies (weakens) the hydrological cycle in that hemisphere, and precipitation increases (decreases). Due to the 20-kyr periodicity of the precessional cycle, when the wet-season occurs at perihelion, 10 kyr later that hemisphere's wet-season must occur at aphelion. This leads to short-term climate extremes; when eccentricity is high, the wettest orbital configuration is followed 10 kyr later by the driest orbital configuration. These 10 kyr climatic swings are reduced when eccentricity declines (i.e. Fig. 6; vertical gray bars).

The wet-season precipitation that dominates cyclothem latitudes is governed by the passage of the ITCZ over the equator and its interaction with the summer monsoon circulation. The seasonal migration of the ITCZ follows the insolation maximum, with the ITCZ reaching its poleward maxima (~10° N and S; Fig. 8) during the summer and winter solstices and passing over the equator during the vernal and autumnal equinoxes. Changes in seasonal ITCZ precipitation intensity are amplified and dampened by eccentricity-modulated, precession-driven temperature variations (Fig. 7). Although cyclothems are located in low, ITCZ influenced latitudes, subtropical to mid-latitude insolation changes play a large role in determining tropical precipitation distributions due to their influence on the summer monsoon strength. In the late Paleozoic northern hemisphere the summer-monsoon low forms at ~20° N and tends to be relatively weak (1005–1010 mb) compared to its southern hemisphere counterpart, which forms at ~40° S and maintains sea-level pressures of 995–1000 mb (Fig. 8a-d). The southern hemisphere monsoon is significantly stronger than that of the northern hemisphere due to the greater distribution of continental landmass located south of the equator (Kutzbach and Gallimore, 1989; Kutzbach, 1994). During the SH summer (Fig. 8a and e), the monsoonal low

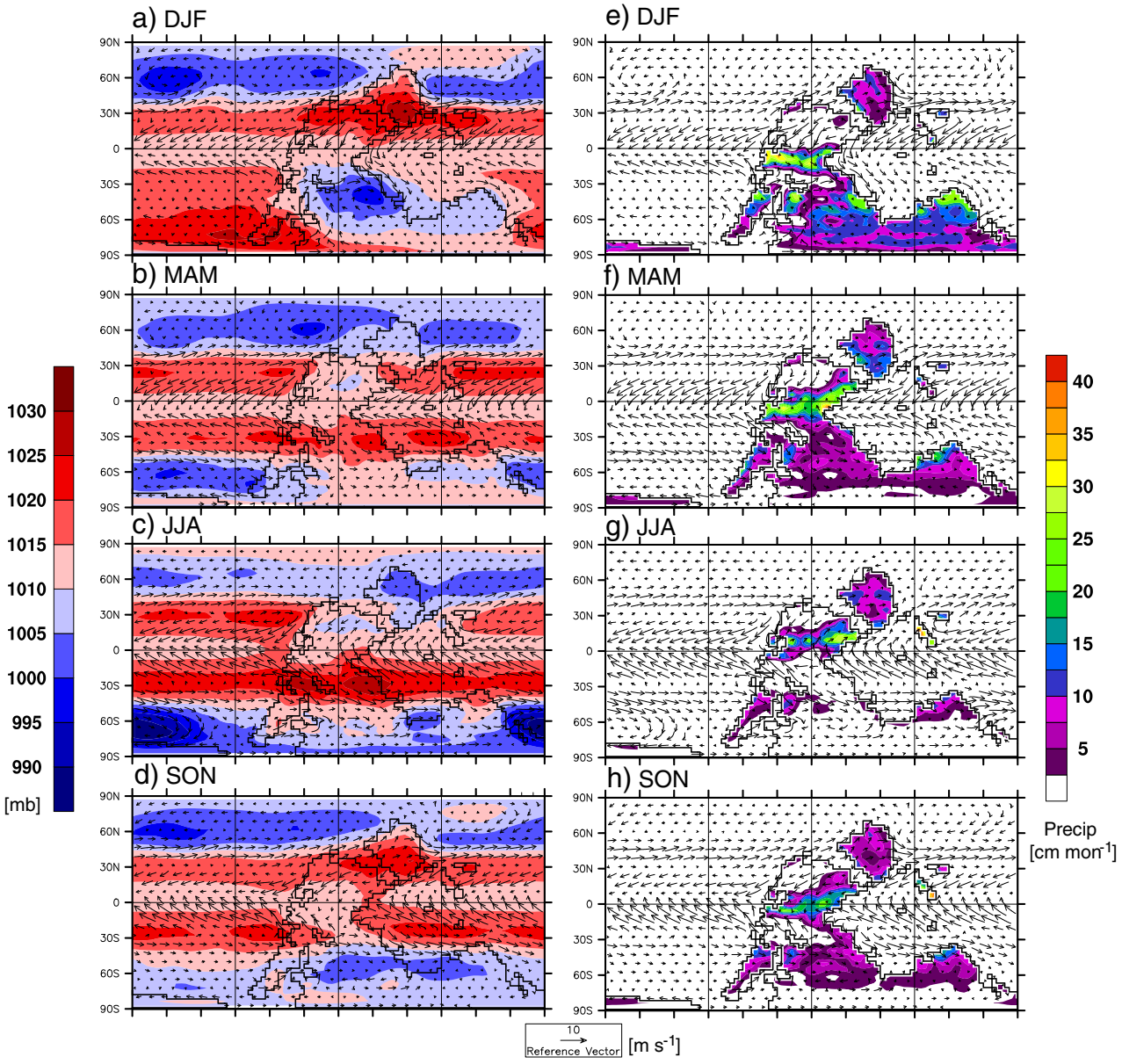

Fig. 8. ITCZ-monsoon interactions. (a–d) Snapshots (65 kyr) of seasonal sea-level pressure [mb] and surface wind speed [m s^{-1}] and direction. Monsoon lows form in the summer hemispheres at ~40° S (a) and 20° N (c). The northern hemisphere monsoon low is notably weaker than its southern hemisphere counterpart. (e-h) Snapshots (65 kyr) of seasonal precipitation [cm mon^{-1}] and winds (precipitation over the ocean has been masked). In the SH summer (e) the monsoon low diverts equatorial on-shore easterly flow toward high latitude Gondwanaland, increasing precipitation along the Paleotethys coast.

diverts equatorial easterlies southward, which decreases low-latitude on-shore moisture-laden flow and reduces tropical precipitation. This diverted moisture increases SH mid-latitude precipitation, particularly along the Paleotethys coast (Fig. 8e). On an annual basis, the result of this diversion is that the NH tropics receive more moisture during the wet season than their SH counterparts (compare a-c with g-i in Fig. 7).

4. Discussion

4.1. Model results summary

The model results presented in this study demonstrate the substantial roles that both atmospheric pCO_2 concentrations and orbital parameter fluctuations play in determining high-latitude Gondwanan glaciation and low-latitude Pangaean climate variability. Our simulations indicate that average low-latitude Pangaean vegetation coverage, mean-annual precipitation, and wet-season length are governed by atmospheric pCO_2 concentration, but that short-term variations in these climatic variables can be driven by orbital insolation fluctuations. We find that the low pCO_2 concentrations conducive to large-scale Gondwanaland glaciation are accompanied by higher mean-annual low-latitude continental precipitation, longer wet-season length, and increased vegetation coverage. High pCO_2 concentrations promote ice-free high latitudes, lower mean-annual low-latitude continental precipitation, shorter wet-season length, and reduced vegetation coverage. Such fluctuations (from140 to 420 ppm and vice versa) in atmospheric pCO_2 concentrations were unlikely to have occurred over short-to-intermediate (10^4–10^5 years) time intervals in the late Paleozoic, but likely played a larger role in the long-term (10^6–10^7 years) evolution of mean climatic states (Montañez et al., 2007; DiMichele et al., 2009).

On orbital time-scales, variations in high-latitude continental ice sheets and low-latitude continental precipitation are paced by the eccentricity of Earth's orbit; when eccentricity is high, precessionally driven temperature changes are amplified and seasonal variability is increased. When eccentricity is low, precessional changes are damped and seasonal variability remains relatively constant. Our experiments indicate that low eccentricity corresponds to climates with stable high-latitude ice volumes and low variability in the seasonal distribution of low-latitude precipitation, whereas high eccentricity produces conditions that are conducive to high-latitude ice-sheet accumulation and ablation as well as seasonally variable low-latitude precipitation distributions. Eccentricity-paced precessional amplification persists for the duration of a season's close pass to the sun (~5 kyrs), thus tropical wet-season (summer and fall) amplification occurs over an ~10 kyr period within each hemisphere. In addition, although our study does not simulate Pleistocene-like (±80–100 ppm) atmospheric pCO_2 fluctuations over glacial–interglacial cycles, our results indicate that if pCO_2 changes accompany eccentricity-modulated glacial cycles, average low-latitude precipitation would decrease during interglacial periods and increase during glacial periods.

In our experiments orbital-scale low-latitude climatic trends are largely unaffected by Gondwanaland ice sheets, but based on both the upward trend in precipitation through time in the 420-ppm experiment (Fig. 6c) and the results of Poulsen et al. (2007) and Peyser and Poulsen (2008), it is reasonable to assume that if ice sheets reached further northward than those simulated, larger changes to tropical precipitation would result. Beyond the direct atmospheric influence of continental ice sheets on climate, ice sheets also regulate global sea level. In our simulations, ice sheets of adequate volume to account for the sea-level fluctuations required of cyclothem deposition models are simulated at atmospheric pCO_2 concentrations of 420 and 560 ppm, but not at 840 ppm. Cyclothem-style fluctuations in ice volume, wherein ice sheets wax and wane with changing orbital insolation, occur only in the 560 ppm simulation and result in ice sheet volume fluctuations equivalent to ~33 m of glacioeustatic change (Fig. 1a). The ice sheet simulated at 420 ppm is resistant to orbitally driven temperature increases due to ice-height and ice-albedo feedbacks (Horton et al., 2010). These results suggest a relatively narrow window ($840 > pCO_2 > 420$) within which orbitally driven glacioeustatic fluctuations are sufficient to develop cyclothems that require moderate (on the order of 33 m) eustatic fluctuations. Successions that require glacioeustatic fluctuations much greater than 33 m, inferred from some late Paleozoic deposits (Heckel, 1977; Soreghan and Giles, 1999; Algeo et al., 2004; Rygel et al., 2008), may require feedbacks not accounted for in our modeling study (i.e., orbital-scale greenhouse gas changes, dust flux, dynamic ocean currents, etc.).

4.2. Influence of eccentricity-paced climate change on deposition

Based on our results, studies that attempt to explain cyclothem facies variations by invoking only ice sheet-induced glacial-interglacial wet-dry (or vice-versa) cycles have by and large oversimplified the causes of tropical climate variability (e.g., Soreghan, 1994; Tandon and Gibling, 1994; Heckel, 1995; Miller et al., 1996; Cecil et al, 2003). Our results indicate that changes in orbital insolation play a substantial role in determining the climate within the depositional environment and must be considered in conjunction with climatic changes brought about by fluctuations in ice sheet volume/eustasy. Our results indicate that within the appropriate pCO_2 window low-latitude climatic changes, high-latitude glacial-interglacial cycles, and glacioeustatic fluctuations are simultaneously driven by variations in orbital insolation. Based on these model results, and the observation that cyclothems display 100 and 400 kyr eccentricity-band periodicities, we discuss the implications of eccentricity-paced precessional changes on cyclic sediment deposition in paleotropical Pangaea, with no specificity to geographic region within this climatic belt. Because many cyclothem facies require changes in eustasy, in addition to much slower rates of thermo-tectonic subsidence, to create accommodation space, our discussion will focus on the 560 ppm pCO_2 simulation, particularly the Orbit 3 segment (161–240 kyr; Fig. 9), due to its glacial-interglacial rhythm, though it should be noted that orbitally-driven low latitude climate changes occur regardless of ice volume variation. For the sake of clarity we focus our discussion on depositional environments located in the Northern Hemisphere and tailor our discussion to the low-slope, ramp-like settings of cratonic platforms and their epicontinental seas (Watney et al., 1989).

We describe conditions in northern hemisphere tropical Pangaea at three points in the glacioeustatic cycle: (A) the highstand of sea level through ice buildup (early glacial stage), (B) the period of maximum accumulation of continental ice (late glacial stage), and (C) the onset of transgression through maximum sea level, initiated by the turnover in eccentricity and driven by ice sheet disintegration (end glacial stage).

A) We begin our discussion at the glacial minima/sea-level highstand to highlight the climatic conditions leading to ice buildup (left side (Early Glacial); Fig. 9). Eccentricity (green curve on Fig. 9) is at a maximum, but is gradually declining. Over the first ten thousand year period (i.e., half the precessional cycle), the combination of low obliquity (yellow curve) and the SH summer and fall seasons at aphelion produce anomalously cool southern latitudes that allow snow to persist throughout the melt season. Ice sheets begin to rapidly accumulate. In the NH tropics, the summer and fall wet-seasons occur at perihelion and mean-annual precipitation is anomalously high. Ten thousand years later, the SH summer and fall occur during perihelion leading to relatively warm high southern latitudes. This warming is countered by increasing obliquity and the newly formed ice sheet's albedo and height feedbacks. The pace of ice sheet growth diminishes. In the NH tropics, the summer and fall wet-seasons occur

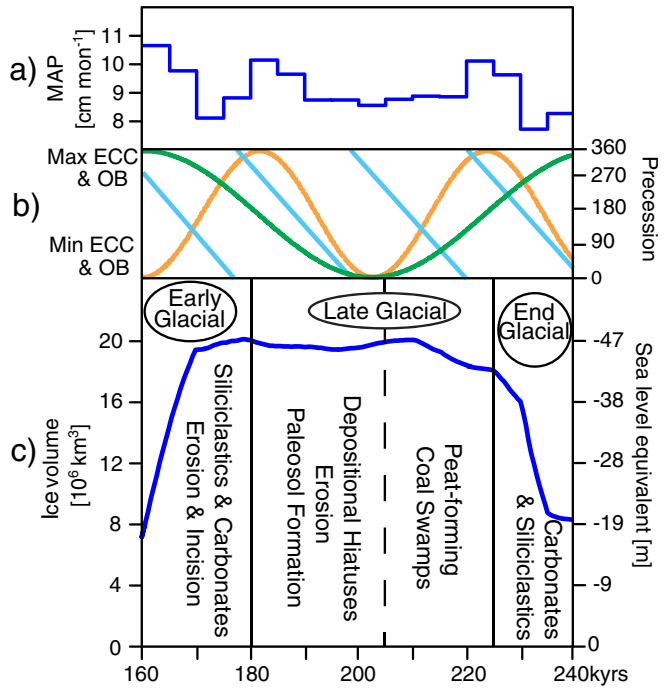

Fig. 9. Time-series of climatic change and the depositional environment for one eccentricity cycle (Orbit 3; 160 to 240 kyr). (a) Northern hemisphere tropical (0°–15° N) continental mean-annual precipitation [cm mon^{-1}] from the 560 ppm simulation. (b) Orbital regime used in simulations (See Fig. 6 caption). (c) Ice volume [10^6 km^3], sea level equivalent [m], and ice sheet phase/low latitude depositional interpretation. Depositional environment interpretations take into account low-latitude climate and the effect of high-latitude ice sheet volume changes on relative sea level. The hiatus-to-coal transition (~205 kyr) is represented by a dashed vertical line to indicate that no change in rate of subsidence v. eustasy is accounted for in this diagram.

at aphelion and mean-annual precipitation is anomalously low. Throughout the ice-accumulation phase, base levels fall within the epieric sea depositional environment.

In this climate scenario, low-latitude precipitation, beginning with maximum stand of sea-level through subsequent ice buildup (early glacial or forced regression phase), is highly variable with a period of ~10 kyr of the wettest tropical orbital configuration of the entire glacial-interglacial cycle followed 10 kyr later by the driest. Aggradation and progradation of regressive limestones (e.g., Midcontinent cyclothems) and/or delta top siliciclastic facies (e.g., Donets Basin) would be followed by fluvial downcutting and erosion on landscapes and development of paleosols with seasonal characteristics (e.g., Vertisols), with the likely development of polygenetic paleosols that record the rapid precessionally-driven precipitation fluctuations.

B) Once eccentricity is low and precessional changes are no longer significantly amplified (middle (Late Glacial); Fig. 9), ice sheets approach their maximum volume and both sea level and eustatic fall rates are at minima (late glacial or late lowstand depositional stage). Precipitation remains seasonal (dominantly distributed during the summer and fall wet-season), but extreme highs and lows are absent at all time-scales from seasonal to precessional. Though the ice sheet has attained a relatively steady state, minor fluctuations in ice volume persist. Given that sea level is at its minimum, this period is dominated initially by erosion, paleosol formation, and depositional hiatuses. During the later part of this period accommodation space increases once the rate of subsidence outpaces that of the eustatic fall. The non-variable distribution of seasonal precipitation throughout this low eccentricity period, in conjunction with increased accommodation space, leads to an elevated water table, stabilization of soil surfaces by vegetation, and the onset of organic accumulation. In total, these conditions promote the expansion of regionally widespread peat-swamp forests and favor the preservation of coal deposits.

C) At the transition from low to high eccentricity modulation, precessional climate changes are increasingly amplified (right side (End Glacial); Fig. 9). The combination of high obliquity and SH spring and summer at perihelion produce anomalously warm high southern latitudes during the melt-season, initiating ice sheet disintegration. Initial marine incursion would lead to a reduction in the areal coverage of widespread wetlands and sediment backfilling of previously incised fluvial valleys with eustuarine deposits and reworked nearshore sands. In the NH tropics, precipitation variability returns with anomalously high precipitation when the NH wet season occurs at perihelion, followed ten thousand years later by anomalously low precipitation when the NH wet season occurs at aphelion. This high climatic variability, including an increase in seasonality, would permit the penetration of seasonal-drought tolerant vegetation into the once wetland covered lowlands and lead to significant compositional change in lowland vegetational cover (DiMichele et al., 2010).

Rapid ice sheet ablation early in the high eccentricity phase (beginning at ~230 kyr in Fig. 9), an increasingly rapid rate of eustatic rise, and the creation of substantial accommodation space permits the accumulation and preservation of a thick sedimentary package of marine carbonates and siliciclastics during this phase of the glacial-interglacial cycle (Watney et al., 1989; Read, 1998). Initial transgressive deposits backfilling fluvial channels and incised valleys would be quickly replaced by marine carbonate and/or black shale deposition, with the point of maximum rate of transgression recorded within these typically anoxic shale deposits (Algeo et al., 2004; Heckel, 2008). The volume of siliciclastics transported down river systems during this transgressive period likely waxed and waned with precessionally driven precipitation swings (Cecil, 1990; Cecil and Dulong, 2003).

4.3. Implications for tropical Pangaean sequences

Cyclothem deposits display significant compositional, regional, and temporal variability and the application of any single depositional model that links climate with eustasy should not be made without considerations (cf. Rankey, 1997). The eccentricity-paced changes in tropical climate and depositional environment that we have discussed cannot account for all cyclothem variability, though such variability may be caused by differences in regional climate, autocyclic depositional processes, periods of non-deposition, and/or complexities inherent to orbital parameter periodicities. For example, in the natural world, orbital parameters have multiple periodicities, each of which varies on an independent timescale. In our simulations we have minimized these complexities; we use an orbital regime that frequently aligns obliquity, eccentricity, and precession such that the parameters combine constructively to create maxima and minima in insolation (DeConto and Pollard, 2003; Horton and Poulsen, 2009). In the naturally evolving climate system, orbital parameters would not combine constructively as frequently as simulated in this study and the patterns of climate change recorded in geological units would display significant lithological and temporal variability, as is the case of cyclothems. In addition, our simplification of the eccentricity cycle from 100 kyrs to 80 kyrs reduces the number of precessional cycles that can operate within a full eccentricity cycle, thereby reducing the amount of variability one would expect to find in the sedimentary record. To further this point, we acknowledge that the time-scale of various stages of ice accumulation and disintegration are an artifact of using end-member orbital parameter values within a compressed period of eccentricity. As such, one should infer that the accumulation and ablation of ice sheets likely occurred over longer periods of time than those depicted in Fig. 9, in fact some have estimated that 50 to 90% of the eccentricity period should be

dominated by ice accumulation/sea-level fall (Watney et al., 1989; Read, 1998). Based on these considerations, we emphasize that the intent of this study is to highlight the mechanistic linkages between orbitally driven climate change and the sedimentary record, and that to do so we have made concessions in the name of computational practicality.

The climate modeling results presented in this study suggest that significant orbital-scale variability in paleo-tropical Pangaean climate may be driven by either atmospheric pCO_2 change or orbital insolation change, though it is probable that these parameters did not change independently. As in the Pleistocene (Petit et al., 1999), orbital insolation changes were likely accompanied by feedbacks that increased/decreased greenhouse gas concentrations and amplified climatic changes. For example, modest fluctuations in atmospheric pCO_2 concentrations ($\pm$80–100 ppm if on the scale of Pleistocene glacial–interglacial fluctuations), coincident with orbital insolation change, could facilitate the expansion and contraction of higher volume Gondwanaland ice sheets, increase the amplitude of glacioeustatic changes, amplify low latitude cycles of aridity and humidity, and promote the exchange/modification of ecosystems.

5. Model caveats and discussion

The application of our simulated climate framework to late Paleozoic observations is not without caveats. The use of Sakmarian paleogeography and paleotopography represents a single moment in the evolution of the late Paleozoic supercontinent. In reality, late Paleozoic cyclothem deposition began 45 myr prior to the Sakmarian and tropical climate dynamics were likely influenced by the evolution of continental landmass distributions (Torsvik and Cocks, 2004) and the evolution of the central Pangaean mountains (Rowley et al., 1985). For example, GCM studies of the late Paleozoic have demonstrated that the addition of a low-latitude mountain range of moderate elevation (3 km) can decrease the seasonality of regional precipitation by creating an anomalous low-pressure center over elevated terrains during the tropical dry-season (Otto-Bliesner, 1993, 2003; Peyser and Poulsen, 2008). We predict that an increase in low-latitude topography could lead to a similar reduction in seasonality in our model, but that the cyclicity observed in cyclothem deposits must be generated by fluctuations in orbital insolation.

The use of a modern ecosystem model (BIOME4) in the simulation of late Paleozoic climate is a limitation, but given the uncertainty inherent in late Paleozoic plant physiology and the lack of a suitable late Paleozoic biome-model alternative, we think it is justified. Late Paleozoic low-latitude ecosystem change has been chronicled on glacial-interglacial time-scales, across ages, and from the start of the Carboniferous to the end of the Permian (DiMichele et al., 2001; Montañez et al., 2007; DiMichele et al., 2009, 2010). These studies attribute both short to intermediate-term cycles of species dominance and long-term floral transitions to changes in late Paleozoic climate. Whereas climate most certainly influenced late Paleozoic floral variations, the reciprocal role of these vegetation fluctuations in influencing LPIA climate is not well understood.

Of particular importance to the study of low-latitude climate is the role that tropical vegetation plays in precipitation distribution. In the modern tropics, rainforest ecosystems are largely comprised of angiosperm vegetation. Angiosperms have substantial transpiration capabilities that are thought to reduce the seasonality of precipitation (Boyce and Lee, 2010). In the late Paleozoic, angiosperms had not yet evolved, but evidence suggests that the transpiration capabilities of some coal-swamp forest vegetation types may have reached the lower range of angiosperm levels (Wilson et al., 2008). Additionally, some types of late Paleozoic wetland plants are thought to have had large total leaf areas (Laveine, 1986) and high growth rates, factors that in aggregate potentially offset decreased transpiration capability on a per-unit of leaf-surface-area basis (Phillips and DiMichele, 1992; Cleal and Thomas, 2005). Although these combined factors suggest that some late Paleozoic vegetation types may be well represented by modern analogs, the degree to which the BIOME 4 ecosystem model appropriately represents late Paleozoic floral ecosystems awaits the integration of late Paleozoic paleobotanical observations into climate models.

6. Conclusion

In this study we utilize a climate model to investigate the processes that drove late Paleozoic climate change and address the effect of these changes on cyclic low-latitude sediment deposition. Our model results demonstrate that both atmospheric pCO_2 concentrations and orbital insolation variations are important factors in determining the volume of high-latitude Pangaean ice sheets and the climatic conditions within low-latitude depositional environments. Our results further indicate that within a narrow atmospheric pCO_2 window ($840 < pCO_2 < 420$) changes in the eccentricity of Earth's orbit paced the accumulation and ablation of Gondwanaland ice sheets, modulated glacioeustatic change, and controlled the distribution of precipitation and vegetation across low-latitude Pangaea. On the basis of these results, we propose that the rhythmic sedimentation patterns observed in Euramerican cyclothem deposits are the result of eccentricity-paced changes in both high and low-latitude late Paleozoic climate.

Supplementary data to this article can be found online at doi:10.1016/j.palaeo.2012.03.014.

Acknowledgements

D.E.H. and C.J.P. were supported by NSF grant EAR-0544760. D.E.H. received additional support from the Rocky Mountain Association of Geologists Veterans Memorial Scholarship. I.P.M. was supported by NSF grant EAR-0545701 and EAR-1024737. We offer our thanks to the members of the Climate Change Research Laboratory at the University of Michigan for inspiring discussions and we thank T. Olszewski and an anonymous reviewer for constructive manuscript reviews.

References

Algeo, T.J., Schwark, L., Hower, J.C., 2004. High-resolution geochemistry and sequence stratigraphy of the Hushpuckney Shale (Swope Formation, eastern Kansas): Implications for climato-environmental dynamics of the Late Pennsylvanian Midcontinent Sea. Chemical Geology 206, 259–288.
Berger, A., Loutre, M.F., 1991. Insolation values for the climate of the last 10,000,000 years. Quaternary Science Reviews 10, 297–317.
Bishop, J.W., Montañez, I.P., Osleger, D.A., 2010. Dynamic carboniferous climate change, Arrow Canyon, Nevada. Geosphere 6, 1–34.
Boyce, C.K., Lee, J.E., 2010. An exceptional role for flowering plant physiology in the expansion of tropical rainforests and biodiversity. Proceedings of the Royal Society B: Biological Sciences 277, 3437–3443.
Caputo, M.V., Crowell, J.C., 1985. Migration of glacial centers across Gondwana during Paleozoic Era. Geological Society of America Bulletin 96, 1020–1036.
Cecil, C.B., 1990. Paleoclimate controls on stratographic repetition of chemical and siliciclatic rocks. Geology 18, 533–536.
Cecil, C.B., Dulong, F.T., 2003. Precipitation models for sediment supply in warm climates. In: Cecil, C.B., Edgar, N.T. (Eds.), *Climate Controls on Stratigraphy*: SEPM Special Publication, 77, pp. 21–27.
Cecil, C.B., Dulong, F.T., West, R.R., Stamm, R., Wardlaw, B., Edgar, N.T., 2003. Climate controls on the stratigraphy of a middle Pennsylvanian cyclothem in North America. In: Cecil, C.B., Edgar, N.T. (Eds.), Climate Controls of Stratigraphy: SEPM Special Publication.
Cleal, C.J., Thomas, B.A., 2005. Paleozoic tropical rainforests and their effect on global climates: is the past the key to the present? Geobiology 3, 13–31.
Crowell, J.C., 1978. Gondwanan Glaciation, Cylothems, Continental Positioning, and Climate Change. American Journal of Science 278, 1345–1372.
DeConto, R.M., Pollard, D., 2003. A coupled-ice seet modeling approach to early Cenozoic history of the Antarctic ice sheet. PPP. 198, 39–52.
DiMichele, W.A., Cecil, B., Montañez, I.P., Falcon-Lang, H., 2010. Cyclic changes in Pennsylvanian paleoclimate and effects on floristic dynamics in tropical Pangaea. International Journal of Coal Geology 83, 329–344.
DiMichele, W.A., Montañez, I.P., Poulsen, C.J., Tabor, N.J., 2009. Climate and vegetational regime shifts in the late Paleozoic ice age earth. Geobiology 7, 200–226.

DiMichele, W.A., Pfefferkorn, H.W., Gastraldo, R.A., 2001. Response of late Carboniferous and Early Permian plant communities to climate change. Annual Review of Earth and Sciences 29, 461–487.
Eros, J.M., Montañez, I.P., Osleger, D.A., Davydov, V.I., Nemyrovska, T.I., Poletaev, V.I., Zhykalyak, M.V., 2012. Upper Carboniferous Sequence Stratigraphy and Relative Sea Level history, Donets Basin. Ukraine, PPP. Palaeogeography, Palaeoclimatology, Palaeoecology. doi:10.1016/j.palaeo.2011.08.019.
Fielding, C.R., Frank, T.D., Birgenheier, L.P., Rygel, M.C., Jones, A.T., Roberts, J., 2008a. Stratigraphic imprint of the Late Paleozoic Ice Age in eastern Australia: a record of alternating glacial and nonglacial climate regimes. Journal of the Geological Society of London 165, 129–140.
Fielding, C.R., Frank, T.D., Isbell, J.I., 2008b. The Late Paleozoic Ice Age-a Review of Current Understanding and Sythesis of Global Climate Patterns. In: Fielding, C.R., Frank, T.D., Isbell, J.I. (Eds.), Resolving the Late Paleozoic Ice Age in Time and Space: Geol. Soc. Am. Spec. Pap., 441.
Gibling, M.R., Rygel, M.C., 2008. Late Paleozoic cyclic strata of Euramerica: Gondwanan glacial signatures enhanced during slow-subsidence periods. In: Fielding, C.R., Frank, T.D., Isbell, J. (Eds.), Resolving the Late Paleozoic Ice Age in Time and Space: Geological Society of America Special Publication, 441, pp. 219–233.
Harrison, S.P., Prentice, A.I., 2003. Climate and CO_2 controls on global vegetation distribution at the last glacial maximum: analysis based on palaeovegetation data, biome modelling and palaeoclimate simulations. Global Change Biology 9, 983–1004.
Heckel, P.H., 1977. Origin of phosphatic black sahel facies in Pennsylvanian cyclothems of Mid-Continent North America. American Association of Petroleum Geologists Bulletin 61, 1045–1068.
Heckel, P.H., 1986. Sea-Level Curve for Pennsylvanian Eustatic Marine Transgressive-Regressive Depositional Cycles Along Midcontinent Outcrop Belt, North-America. Geology 14, 330–334.
Heckel, P.H., 1995. Glacial-eustatic base-level-Climatic model for late middle to late Pennsylvanian coal-bed formation in the Appalachian basin. Journal of Sedimentary Research B65, 348–356.
Heckel, P.H., 2008. Pennsylvanian cyclothems in Midcontinent North America as far-field effects of waxing and waning of Gondwana ice sheets. In: Fielding, C.R., Frank, T.D., Isbell, J.L. (Eds.), Resolving the late Paleozoic ice age in time and space: GSA Special Paper, 441, pp. 275–289.
Horton, D.E., Poulsen, C.J., 2009. Paradox of late Paleozoic glacioeustasy. Geology 37, 715–718.
Horton, D.E., Poulsen, C.J., Pollard, D., 2007. Orbital and CO_2 forcing of late Paleozoic continental ice sheets. Geophysical Research Letters 34, L19708.
Horton, D.E., Poulsen, C.J., Pollard, D., 2010. Influence of high-latitude vegetation feedbacks on late Palaeozoic glacial cycles. Nature Geoscience 3, 572–577.
Imbrie, J., Imbrie, J.Z., 1980. Modeling the Climatic Response to Orbital Variations. Science 207, 943–953.
Isbell, J.L., Miller, M.F., Wolfe, K.L., Lenaker, P.A., 2003. Timing of late Paleozoic glaciation in Gondwana: Was glaciation responsible for the development of Northern Hemisphere cyclothems? In: Chan, M.A., Archer, A.W. (Eds.), Extreme Depositional Environments: Mega End Members in Geologic Time. Spec, Pap. Geol. Soc. Am., pp. 5–24.
Kaplan, J.O., Bigelow, N.H., Prentice, I.C., Harrison, S.P., Bartlein, P.J., Christensen, T.R., Cramer, W., Matveyeva, N.V., McGuire, A.D., Murray, D.F., Razzhivin, V.Y., Smith, B., Walker, D.A., Anderson, P.M., Andreev, A.A., Brubaker, L.B., Edwards, M.E., Lozhkin, A.V., 2003. Climate change and Arctic ecosystems: 2. Modeling, paleodata-model comparisons, and future projections. Journal of Geophysical Research-Atmospheres 108.
Kutzbach, J.E., 1994. Idealized Pangean climates: Sensitivity to orbital change. In: Klein, G.D. (Ed.), Pangea: Paleoclimate, Tectonics, and Sedimentation during Accretion, Zenith, and Breakup of a Supercontinent. Geological Society of America, Boulder, CO, pp. 41–55.
Kutzbach, J.E., Gallimore, R.G., 1989. Pangaean Climates - Megamonsoons of the Megacontinent. Journal of Geophysical Research-Atmospheres 94, 3341–3357.
Laveine, J., 1986. The size of the frond in the genus *Alethopteris* STERNBERG (Pteridospermopsida, Carboniferous). Geobios-Lyon 19, 49–59.
Martin, L., Montañez, I.P., Bishop, J., 2012. Carboniferous sequence stratigraphy and sea-level history of the Bird Spring platform, Southern Great Basin, USA. Palaeogeography, Palaeoclimatology, Palaeoecology. doi:10.1016/j.palaeo.2012.02.018.
Miller, K.B., McCahon, T.J., West, R.R., 1996. Lower Permian (Wolfcampian) paleosol-bearing cycles of the US midcontinent: Evidence of climatic cyclicity. Journal of Sedimentary Research 66, 71–84.
Montañez, I.P., Tabor, N.J., Niemeier, D., DiMichele, W.A., Frank, T.D., Fielding, C.R., Isbell, J.L., Birgenheier, L.P., Rygel, M.C., 2007. CO_2-forced climate and vegetation instability during late paleozoic deglaciation. Science 315, 87–91.
Otto-Bliesner, B., 1993. Tropical mountains and coal formation: A climate model study of the Westphalian (306 Ma). Geophycical Research Letters 20, 1947–1950.
Otto-Bliesner, B., 2003. The role of mountains, polar ice, and vegetation in determining the tropical climate during the middle Pennsylvanian: climate model simulations. In: Cecil, C.B., Edgar, N.T. (Eds.), Climate Controls of Stratigraphy: SEPM Special Publication No. 77, pp. 227–237.
Petit, J.R., Jouzel, J., Raynaud, D., Barkov, N.I., Barnola, J.M., Basile, I., Bender, M., Chappellaz, J., Davis, M., Delaygue, G., Delmotte, M., Kotlyakov, V.M., Legrand, M., Lipenkov, V.Y., Lorius, C., Pepin, L., Ritz, C., Saltzman, E., Stievenard, M., 1999. Climate and atmospheric history of the past 420,000 years from the Vostok ice core, Antarctica. Nature 399, 429–436.
Peyser, C.E., Poulsen, C.J., 2008. Controls on Permo-Carboniferous precipitation over tropical Pangaea: A GCM sensitivity study. Palaeogeography, Palaeoclimatology, Palaeoecology 268, 181–192.
Phillips, T.L., DiMichele, W.A., 1992. Comparative ecology and life history biology of arborescent lycopods in Late Carboniferous swamps of Euramerica. Annals of the Missouri Botanical Garden 79, 560–588.
Pollard, D., Thompson, S.L., 1995. Use of a Land-Surface-Transfer Scheme (Lsx) in a Global Climate Model - the Response to Doubling Stomatal-Resistance. Global Planet Change 10, 129–161.
Poulsen, C.J., Pollard, D., Montañez, I.P., Rowley, D., 2007. Late Paleozoic tropical climate response to Gondwanan deglaciation. Geology 35, 771–774.
Rankey, E.C., 1997. Relations between relative changes in sea level and climate shifts: Pennsylvanian-Permian mixed carbonate-siliciclastic strata, western United States. GSA Bulletin 109, 1089–1100.
Read, J.F., 1998. Phanerozoic carbonate ramps from greenhouse, transitional and ice-house worlds: clues from field and modeling studies. In: Wright, V.P., Burchette, T.P. (Eds.), Carbonate Ramps: Geological Society Special Publications, 149, pp. 107–135.
Rowley, D.B., Raymond, A., Parrish, J.T., Lottes, A.L., Scotese, C.R., Ziegler, A.M., 1985. Carboniferous Paleogeographic, Phytogeographic, and Paleoclimatic Reconstructions. International Journal of Coal Geology 5, 7–42.
Rygel, M.C., Fielding, C.R., Frank, T.D., Birgenheier, L.P., 2008. The magnitude of late Paleozoic glacioeustatic fluctuations: a synthesis. Journal of Sedimentary Research 78, 500–511.
Soreghan, G.S., 1994. The impact of glacioclimatic change on Pennsylvanian cyclostratigraphy. In: Embry, A.F., Beauchamp, B., Glass, D.J. (Eds.), Pangea–Global environments and resources: Canadian Society of Petroleum Geologists Memoir, pp. 523–543.
Soreghan, G.S., Giles, K.A., 1999. Amplitudes of Late Pennsylvanian glacioeustasy. Geology 27, 255–258.
Strömberg, C.A.E., 2005. Decoupled taxonomic radiation and ecological expansion of open-habitat grasses in the Cenozoic of North America. Proceedings of the National Academy of Science United States of America 102, 11980–11984.
Tandon, S.K., Gibling, M.R., 1994. Calcrete and Coal in Late Carboniferous Cyclotherms of Nova-Scotia, Canada - Climate and Sea-Level Changes Linked. Geology 22, 755–758.
Thompson, S.L., Pollard, D., 1995. A Global Climate Model (Genesis) with a Land-Surface Transfer Scheme (Lsx).1. Present Climate Simulation. Journal of Climate 8, 732–761.
Thompson, S.L., Pollard, D., 1997. Greenland and Antarctic mass balances for present and doubled atmospheric CO_2 from the GENESIS version-2 global climate model. Journal of Climate 10, 871–900.
Torsvik, T.H., Cocks, L.R.M., 2004. Earth geography from 400 to 250 Ma: a palaeomagnetic, faunal and facies review. Journal of the Geological Society of London 161, 555–572.
Watney, W.L., Wong, J.-C., French Jr., J.A., 1989. Computer simulation of Upper Pennsylvanian (Missourian) carbonate-dominated cycles in western Kansas. In: Franseen, E.K., Watney, W.L., Kendall, C.G.St.C., Ross, W. (Eds.), Sedimentary Modeling: Computer simulations and methods for improved parameter definition: Kansas Geological Survey Bull., 233, pp. 415–430.
Wilson, J.P., Knoll, A.H., Holbrook, N.M., Marshall, C.R., 2008. Modeling fluid flow in Medullosa, an anatomically unusual Carboniferous seed plant. Paleobiology 34, 472–493.
Ziegler, A.M., Hulver, M.L., Rowley, D.B., 1997. Permian world topography and climate. In: Martini, I.P. (Ed.), Late Glacial and Post- glacial Environmental Changes—Quaternary, Carboniferous-Permian and Proterozoic. Oxford University Press, New York, pp. 111–146.

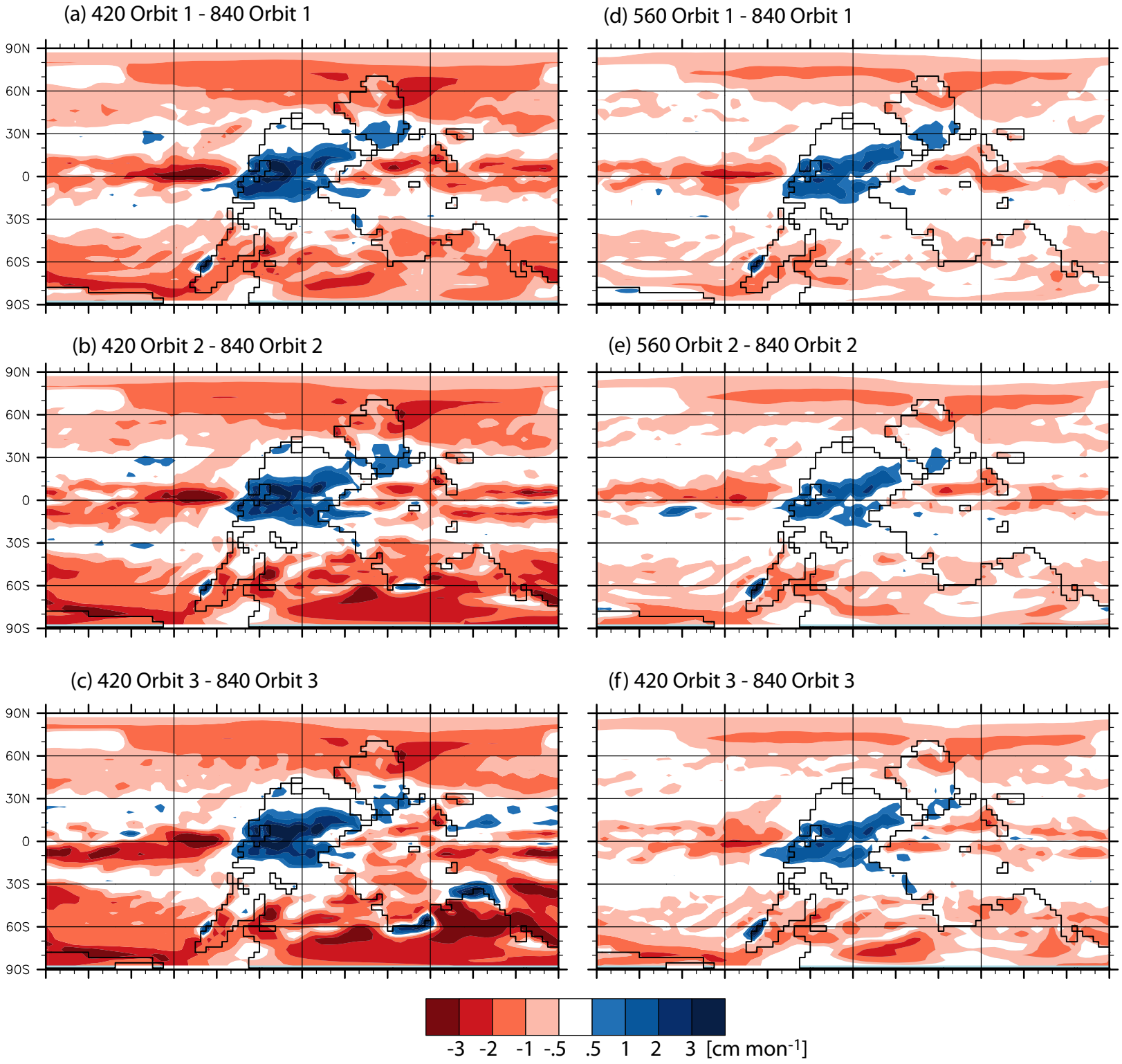
(a) 420 Orbit 1 - 840 Orbit 1
(d) 560 Orbit 1 - 840 Orbit 1
(b) 420 Orbit 2 - 840 Orbit 2
(e) 560 Orbit 2 - 840 Orbit 2
(c) 420 Orbit 3 - 840 Orbit 3
(f) 420 Orbit 3 - 840 Orbit 3
90N
60N
30N
0
30S
60S
90S
-3 -2 -1 -.5 .5 1 2 3 [cm mon-1]